HHS Public Access

Author manuscript

Invest Ophthalmol Vis Sci. Author manuscript; available in PMC 2015 July 17.

Published in final edited form as:

Invest Ophthalmol Vis Sci. 2005 June ; 46(6): 2156–2167. doi:10.1167/iovs.04-1427.

Cone-like Morphological, Molecular, and Electrophysiological Features of the Photoreceptors of the *Nrl* Knockout Mouse

Lauren L. Daniele[1], **Concepcion Lillo**[2,3], **Arkady L. Lyubarsky**[1], **Sergei S. Nikonov**[1], **Nancy Philp**[4], **Alan J. Mears**[5,6], **Anand Swaroop**[5,7], **David S. Williams**[2,3], and **Edward N. Pugh Jr.**[1]

[1]F. M. Kirby Center for Molecular Ophthalmology, Department of Ophthalmology, School of Medicine, University of Pennsylvania, Philadelphia, Pennsylvania

[2]Department of Pharmacology, School of Medicine, University of California, San Diego, California

[3]Department of Neuroscience, School of Medicine, University of California, San Diego, California

[4]Department of Pathology, Anatomy and Cell Biology, Thomas Jefferson University, Philadelphia, Pennsylvania

[5]Department of Ophthalmology and Visual Sciences, University of Michigan, Ann Arbor, Michigan.

[7]Department of Human Genetics, University of Michigan, Ann Arbor, Michigan.

Abstract

Purpose—To test the hypothesis that $Nrl^{-/-}$ photoreceptors are cones, by comparing them with WT rods and cones using morphological, molecular, histochemical, and electrophysio-logical criteria.

Methods—The photoreceptor layer of fixed retinal tissue of 4-to 6-week-old mice was examined in plastic sections by electron microscopy, and by confocal microscopy in frozen sections immunolabeled for the mouse UV-cone pigment and colabeled with PNA. Quantitative immunoblot analysis was used to determine the levels of expression of key cone-specific proteins. Single- and paired-flash methods were used to extract the spectral sensitivity, kinetics, and amplification of the a-wave of the ERG.

Results—Outer segments of $Nrl^{-/-}$ photoreceptors (~7 μm) are shorter than those of wild-type (WT) rods (~25 μm) and cones (~15 μm); but, like WT cones, they have 25 or more basal discs open to the extracellular space, extracellular matrix sheaths stained by PNA, chromatin "clumping" in their nuclei, and mitochondria two times shorter than rods. $Nrl^{-/-}$ photoreceptors express the mouse UV cone pigment, cone transducin, and cone arrestin in amounts expected, given the relative size and density of cones in the two retinas. The ERG a-wave was used to assay the properties of the photocurrent response. The sensitivity of the $Nrl^{-/-}$ a-wave is at its maximum at 360 nm, with a secondary mode at 510 nm having approximately one-tenth the maximum

Corresponding author: Edward N. Pugh, Jr, F. M. Kirby Center for Molecular Ophthalmology, University of Pennsylvania, School of Medicine, 309B Stellar-Chance Bldg., 422 Curie Boulevard, Philadelphia, PA 19104-6069; pugh@mail.med.upenn.edu..

[6]Present affiliation: University of Ottawa Eye Institute, Ottawa Health Research Institute, Ottawa, Ontario, Canada.

Disclosure: **L.L. Daniele**, None; **C. Lillo**, None; **A.L. Lyubarsky**, None; **S.S. Nikonov**, None; **N. Philp**, None; **A.J. Mears**, None; **A. Swaroop**, None; **D.S. Williams**, None; **E.N. Pugh, Jr**, None

sensitivity. These wavelengths are the λ_{max} of the two mouse cone pigments. The time to peak of the dim-flash photocurrent response was ~50 ms, more than two times faster than that of rods.

Conclusions—Many morphological, molecular, and electrophys iological features of the *Nrl*$^{-/-}$ photoreceptors are cone-like, and strongly distinguish these cells from rods. This retina provides a model for the investigation of cone function and cone-specific genetic disease.

The neural retina leucine zipper (*Nrl*) gene encodes a Maf-family transcription factor that regulates the expression of several rod photoreceptor genes.[1–3] Missense mutations in *NRL* are associated with autosomal dominant retinitis pigmentosa in humans.[4] Deletion of *Nrl* in mice (*Nrl*$^{-/-}$) results in the complete absence of rods in the retina, as revealed by histology, immunocytochemistry, electrophysiology, and gene expression analysis. Instead, there is a concomitant increase in short-wave–sensitive photoreceptor cells, apparently generated by switching of rod to cone cell fate during development.[5] In the absence of Nrl, the mouse retina lacks a scotopic response and has a short-wavelength sensitivity enhanced sixfold in its photopic electroretinogram.[5] These results suggest that the *Nrl*$^{-/-}$ mouse may be a useful mammalian model for the investigation of cone function, cone biochemistry, and cone-specific disease, but the initial investigation proposed that *Nrl*$^{-/-}$ photoreceptors are cone–rod intermediates (or “cods”), which function as cones but do not elaborate their full differentiation program.[5] The potential of the *Nrl*$^{-/-}$ mouse as a preparation for the investigation of cone function and disease cannot be fully realized until the classification of the *Nrl*$^{-/-}$ photoreceptors is resolved.

To make a definitive characterization of *Nrl*$^{-/-}$ photoreceptors, we undertook a thorough analysis of the photoreceptor layer of the *Nrl*$^{-/-}$ mouse with light and electron microscopy, of the levels of proteins known to be expressed specifically in cones, and of the electrical responses of the photoreceptors in vivo by using single- and paired-flash methods to record and analyze the a-wave of the ERG. The comparison with results from WT mice showed *Nrl*$^{-/-}$ photoreceptors to exhibit a large set of molecular, ultrastructural, histochemical, and kinetic features highly distinct from the corresponding features of WT rods, but which correspond, with noted exceptions, to the features of WT cones.

Materials and Methods

Animals and General Experimental Methods

All experiments were performed in compliance with National Institutes of Health guidelines, as approved by the Institutional Animal Care and Use Committees of the University of Pennsylvania, and the authors further confirm their adherence to the ARVO Statement for the Use of Animals in Ophthalmic and Vision Research. *Nrl*$^{-/-}$ breeders were generated at the University of Michigan[5] and the offspring produced at the University of Pennsylvania. Animals used for recordings were born and maintained in controlled ambient illumination on a 12-hour light/dark cycle, with an illumination level of 2 to 3 lux. Unless otherwise specified, the age of the animals from which results are reported was 4 to 6 weeks. Our results revealed this to be the age of *Nrl*$^{-/-}$ mice when the saturated amplitude of the a-wave, which is proportional to the massed circulating current of the photoreceptors, is at its

maximum (reviewed in Ref. 6). Wild-type animals were C57Bl/6 and were produced in our facility by pregnant females obtained from Charles River (Wilmington, MA).

Light and Electron Microscopy

Retinas were fixed by perfusion of the whole animal with 2% glutaraldehyde+2% paraformaldehyde in 0.1 M cacodylate buffer (pH 7.4) and embedded in Epon 812. Semithin sections (0.7 μm, stained with toluidine blue) and ultrathin sections were analyzed by light and electron microscopy, respectively.[7,8]

Histochemistry

Mice were euthanatized by overdose of anesthetic and fixed by cardiac perfusion with 4% paraformaldehyde (Electron Microscopy Sciences, Hatfield, PA) in PBS or 4% paraformaldehyde and 0.5% glutaraldehyde/PBS (Sigma-Aldrich, St. Louis, MO). Eyes were dissected from perfused mice with a fine blade and forceps and placed in the fixation solution. Eyecups or whole eyes were placed in 30% sucrose and PBS overnight. Cryosections of 6- to 20-μm thickness were made from mouse eyes embedded in optimal cutting temperature compound (Tissue Tek; Sakura Finetek, Torrance, CA). Sections were washed with PBS and incubated in 1:5000 rabbit anti-mouse UV opsin[9] and 100 μg/mL biotinylated peanut agglutinin (PNA; Vector Laboratories, Burlingame, CA). Additional probes used were goat anti-rabbit antibody conjugated to Alexa-Fluor 555, and avidin-Alexa Fluor 488 (Molecular Probes, Eugene, OR). The buffer used for incubation with primary and secondary antibodies was 0.5% BSA, 0.1% NaN_3, and 0.1% Triton X-100 in PBS.

Quantitative Immunoblot Analysis

To quantify the total MUV per *Nrl*$^{-/-}$ eye, the eyes were enucleated from freshly euthanatized mice and collected in 1.5-mL centrifuge tubes, snap frozen, and stored at −80°C. Mouse cone ultraviolet (MUV) pigment was extracted from frozen *Nrl*$^{-/-}$ eyes according to a published method.[10] Measured quantities of the extract were loaded along with measured quantities of recombinant MUV (described in the next section) on precast Tris-glycine 4% to 12% gels (Invitrogen, Carlsbad, CA), transferred to polyvinylidene difluoride (PVDF) membranes (Immobilon-P; Millipore, Billerica, MA), and blocked with 5% milk and 0.1% Tween in PBS. The membranes were incubated with primary antibodies overnight at 4°C in PBS containing 1% milk and 0.1% Tween. The membranes were then washed in PBS with 0.1% Tween. Secondary antibodies were alkaline phosphatase-conjugated goat anti-rabbit IgG. Chemiluminescence was used to detect the signal (ECL; Amersham Biosciences, Piscataway, NJ), and the band intensities were quantified. (ImageQuant software and the Storm Phosphorimager; Molecular Dynamics, Amersham Biosciences).

For estimation of the relative quantities of $G_t\alpha 2$ (Gnat2) and mCarr (mouse cone arrestin) in *Nrl*$^{-/-}$ versus WT retinas, we used a slightly modified method. Briefly, a frozen eye was thawed, the lens removed through a slit in the cornea, and the eye cut into pieces in a digestion solution consisting of 3% SDS in 0.1 M Tris buffer (pH 6.8). The tissue was homogenized in a measured volume (400–800 μL) of digestion solution in a 1.5-mL centrifuge tube and then centrifuged at 14,000 rpm for 5 minutes. The supernatant was

reserved, and the pellet was resuspended in 100 μL digestion solution and centrifuged again. The total reserved supernatant was combined with 2× Laemmli buffer. Before combining the reserved supernatant with Laemmli buffer, we estimated the total protein in the digested samples with a modified Lowry assay kit (DC Protein Assay; Bio-Rad, Hercules, CA), using dilutions of BSA as the standard. The total protein per eye extracted with this method was estimated to be 0.7 ± 0.08 mg/eye for WT and 0.7 ± 0.09 mg/eye for *Nrl*$^{-/-}$. Samples equated for protein mass were run on precast Tris-glycine 4% to 12% gels (Invitrogen). Polyclonal antibodies used for immunoblotting were rabbit anti-mouse cone arrestin and rabbit anti-clone transducin alpha (Santa Cruz Biotechnology, Santa Cruz, CA). The remaining steps were identical with those used for quantifying MUV pigment.

Recombinant Mouse Cone Ultraviolet Pigment

Purified, recombinant MUV was obtained from Barry Knox (SUNY Upstate Medical Center, Syracuse, NY). MUV, modified with an epitope tag for purification, was expressed in COS1 cells and purified.[11] The purified protein was treated with Peptide N-glycosidase (PNgase; Sigma-Aldrich) before use in quantitative immunoblot analysis.[12] Because MUV complexed with 11-*cis* retinal has its peak α-band absorbance at λ_{max} = 365 nm, close to the absorbance maxima of 11-*cis* retinal (used to generate functional MUV) and to all-*trans* retinal (the bleaching product), it is not possible to quantify MUV at room temperature by bleaching difference spectroscopy. Thus, we quantified purified, re-combinant MUV by its absorbance at 280, assuming an extinction coefficient ε_{280} = 78,000 cm^2/mmol. Absorbance at 280 nm protein is completely determined by the aromatic amino acids content, with extinctions at 280 that can be summed to predict the total.[13] For purified bovine rhodopsin with 31 Phe, 16 Tyr, 5 Trp, the ratio $\varepsilon_{280}/\varepsilon_{500}$ = 1.6 is measured, and so ε_{280} = 67,000.[14] Because MUV (32 Phe, 16 Tyr, 7 Trp) has two more Trps than rhodopsin, each with ε_{280} = 5,600, we obtained the estimate for ε_{280} = 78,000 for MUV.

Electroretinographic Methods

Electroretinograms were recorded, and the a-wave component analyzed, as described previously.[15–17] The only change in the ERG methods from previous publications is that the reference electrode was placed in the mouth instead of being inserted under the skin of the forehead. This conductive “bite bar” served the dual function of acting as the reference and holding the animal's head in a fixed location. It also contributed to an increase in the amplitudes of various ERG components, by 30% to 40%. Both single-flash and paired-flash stimulation protocols were used, the former to estimate the amplification of the activation phase of phototransduction in *Nrl*$^{-/-}$ photoreceptors, and the latter to derive the kinetics of the entire flash response.

Light Stimuli and Calibrations

Light stimuli in the ERG experiments were brief (~1 ms) flashes generated by xenon flash lamps, delivered in a multiport, customized Ganzfeld through calibrated filters.[15] The flashes were monochromatic except for that used to generate an a-wave response of saturating amplitude, which was white (unfiltered). The intensities of the monochromatic

flashes were measured at the plane occupied by the pupil of the mouse in the Ganzfeld with a calibrated photodiode and expressed in photons per square micrometer at the cornea.[15]

Estimation of Amplification by *Nrl*$^{-/-}$ Photoreceptors

Amplification is a fundamental feature of the activation phase of the vertebrate photoreceptor response. Analysis of the cascade has yielded a model that accounts quantitatively for its amplification in terms of the molecular components of the underlying GPCR cascade.[18–20] An analytic approximation of the model is provided by the expression:

$$\begin{aligned} F(t) &= 1, \quad t<t_{eff}; \\ &= epx\left[-\tfrac{1}{2}\Phi A(t-t_{eff})^2\right], \quad t \geq t_{eff} \end{aligned} \quad (1)$$

where $F(t)$ is the fraction of the photoreceptor circulating current present at time t after a flash that produces Φ photoisomerizations per photoreceptor, t_{eff} is a brief delay (a few ms), and A is the amplification constant or coefficient, characteristic of the photoreceptor. The model has been applied in numerous single-cell and electroretinographic (a-wave) investigations to extract the amplification constant (A), which serves as a useful metric of photoreceptor function.[21] When applied to a-wave data, $F(t)$ is estimated as $1 - (a(t)/a_{\text{max}})$, where $a(t)$ is the a-wave and a_{max} its saturating amplitude. Herein, we compare the amplification constant A estimated by applying a published model[1] to ERG a-waves generated by the rods of WT mice and by the photoreceptors of *Nrl*$^{-/-}$ mice. In applying the model, we used a modification of a method[22] that explicitly incorporates the membrane time constant τ_{m} of the cell, in effect, convolving equation 1 with an RC filter with a 1-ms time constant. For the rod a-wave of WT mice, we fixed τ_{m} = 1.0 ms, consistent with previous investigations of the mammalian rod a-wave (e.g., τ_{m} = 1.2 ms[22]; for the a-wave of *Nrl*$^{-/-}$ mice we found that τ_{m} = 2.0 ms provided a good description).

The determination of A requires that flash intensities be expressed in photoisomerizations. An approach, applicable to monochromatic Ganzfeld stimulation in vivo,[15] is captured in the following expression:

$$\Phi = Q(\lambda)\,\tau(\lambda)\,\frac{S_{\text{pupil}}}{S_{\text{retina}}}\,a_{\text{c,end-on}}(\lambda) = Q(\lambda)\quad a_{\text{c,cornea}}\quad(\lambda). \quad (2)$$

In equation 2, Φ is the estimated average number of photoisomerizations produced by a flash of intensity Q photons per square micrometer (measured at the cornea) and wavelength λ; $\tau(\lambda)$, the transmission of the ocular media distal to the outer segments; S_{pupil}, the area of the pupil; S_{retina}, the surface area of the retina at the photoreceptor layer; and $a_{\text{c,end-on}}(\lambda)$ the end-on collecting area of a single photoreceptor at the retina. Collapsing all the factors in equation 2 multiplying the flash intensity $Q(\lambda)$ into a single parameter, one obtains a composite parameter, $a_{\text{c,cornea}}(\lambda)$, which can be thought of as the effective collecting area of the photoreceptor at the cornea in a Ganzfeld. We previously estimated $a_{\text{c,end-on}}(\lambda)$ and $a_{\text{c,cornea}}(\lambda)$ for mouse rods and cones to analyze the sensitivity of components of the ERG,[15,17] but recently updated the estimates for rods by comparing the derived values with the measured rate of rhodopsin bleaching in the Ganzfeld.[23] For WT rods illuminated in vivo, the updated estimates are $a_{\text{c,end-on}}$ = 0.87 μm^2, $a_{\text{c,cornea}}$ = 0.11 μm^2, at the λ_{max} (498

nm) of mouse rhodopsin. To estimate the end-on collecting area of the *Nrl*$^{-/-}$ photoreceptors, the simplest approach would be to assume that their collecting area scales relative to that of rods according to their OS volume ratio, which electron microscopy data presented herein show to be 1:4.3. However, there is a long history of investigations showing that all vertebrate photoreceptors guide or "funnel" light, and that funneling begins in the ellipsoid region of the inner segment, which is invariably larger in diameter than the outer segment, especially in cones.[24,25] The collecting area of turtle cone outer segments, for example, is increased ~30-fold by light funneling in the inner segment.[26] Electron microscopy data presented herein show that *Nrl*$^{-/-}$ photoreceptors, like WT cones, have ellipsoids wider in diameter than their OSs by twofold or more. Assuming these ellipsoids guide light, they should increase the end-on collecting area of *Nrl*$^{-/-}$ photoreceptors by at least fourfold.

Thus, the 4.3-fold smaller OS volume of *Nrl*$^{-/-}$ photoreceptors relative to rods may be compensated by a roughly 4-fold contribution by light funneling, with the result that the effective end-on collecting area of *Nrl*$^{-/-}$ photoreceptors may be about the same as that of WT rods: $a_{c,end\text{-}on}$ = 0.87 μm^2, $a_{c,cornea}$ = 0.11 μm^2 at the λ_{max} (360 nm) for *Nrl*$^{-/-}$ photoreceptors. Although the light funneling factor cannot be considered precise, comparison of ERG results we present with suction electrode results presented elsewhere suggest that it does indeed contribute in the manner proposed.[27]

Results

Structural Characterization of the Photoreceptor Layer and Photoreceptors of the *Nrl*$^{-/-}$ Retina

As visualized with light microscopy in thin plastic sections (Fig. 1), the photoreceptor layer of the *Nrl*$^{-/-}$ retina differs from that of the WT retina in a major respect, the thickness of the outer segment (OS) layer. In the *Nrl*$^{-/-}$, the OS layer is approximately 10 μm thick, about one-third the thickness of the OS layer in the WT retina. Additional differences noted at this scale are a less regular stacking of the outer nuclear layer (ONL) nuclei, and the presence of "rosettes" of ONL nuclei,[5] described in more detail later. Almost all the nuclei in the ONL exhibit a pattern of staining whereby two or more "clumps" of darkly staining chromatin are surrounded by a paler region, a pattern characteristic of WT mouse cone (but not rod) photoreceptor nuclei.[28] The nuclei of cells in the ONL layer of the *Nrl*$^{-/-}$ are larger, less regular in shape, and (perhaps because of their larger volume) have a lower volume density than the smaller, nearly spherical rod nuclei of the WT retina, whose ONL has nearly the same thickness. The lower volume density of nuclei in the ONL layer of the *Nrl*$^{-/-}$ may arise in part from stout myoids that can be seen joining nuclei deeper in the ONL to their inner segments. We attempted to estimate from images such as those in Figure 1 the relative density of nuclei in the retinas of *Nrl*$^{-/-}$ and WT retinas. Although the numbers must be considered preliminary until serial sections from different sectors of the retina are quantified, the analysis suggests that *Nrl*$^{-/-}$ retinas of 4- to 6-week-old mice have fewer ONL nuclei than those of WT control animals, reduced to ~60% of the WT number.

Other distinctive features of the *Nrl*$^{-/-}$ photoreceptors and the OS layer were seen with electron microscopy (Fig. 2). One such feature is the size of the mitochondria, which

resemble those of WT cones, and are highly distinct from the longer, more slender mitochondria of the rods (Table 1).[28] The OS layer of the *Nrl*$^{-/-}$ retina is not so well ordered as that of the WT, and neighboring OSs may project from the IS to the RPE at various angles, and moreover may twist in orientation, unlike the highly parallel projection of the palisade of rod OSs in the WT retina (Fig. 1 in Ref. 28 for electron microscopy data from WT mouse photoreceptors). Measured in images in which it was possible to discern their entirety, the average length of the *Nrl*$^{-/-}$ photoreceptor OSs was 7.3 ± 1.3 μm (n = 21 OSs from five mice; mean ± SD), and the average OS diameter, estimated by measurement at the middle of the OS length, was 1.2 ± 0.3 μm (n = 21; Figs. 2A, 2B). The microvillous projections of the apical membrane of the RPE cells were found to extend into the OS layer 50% or more of its thickness and to encompass completely the shorter OSs. In considering this apparent disorder, it should be kept in mind that the outermost 5 to 7 μm of the OS layer of the WT mouse, into which the apical process of the RPE cells project, can also exhibit considerable disorder (see Fig. 6 in Ref. 28). Thus, the absence of rods in the OS layer of the *Nrl*$^{-/-}$ retina, which places most of the length of the OSs in juxtaposition to the RPE apical surface and its projections, may be a factor affecting the order of the layer.

Another distinctive feature of the *Nrl*$^{-/-}$ photoreceptors was seen at the highest magnification. Up to 30 basal discs of *Nrl*$^{-/-}$ photoreceptors are open to the extracellular space (Fig. 2G–2J). This feature is shared with WT cones, but distinct from the organization of the disc membranes of WT rods, in which the number of open discs is five to seven.[28] It should be noted in this context that in the WT mouse (and in other mammals) cone discs are not fully open to the extracellular space throughout the whole length of the OS.[7,28,29]

In summary, structural and ultrastructural features of the *Nrl*$^{-/-}$ photoreceptors, including the irregularly clumped heterochromatin in their nuclei, the size and shape of their mitochondria and the number of basal discs open to the extracellular spaces, are shared with WT murine cones and are distinct from the corresponding properties of rods.

Binding of PNA to *Nrl*$^{-/-}$ Photoreceptors' Sheaths

The outer and inner segments of mammalian cone (but not rod) photoreceptors are circumscribed by a highly distinct feature of the interphotoreceptor matrix, the "cone sheath,"[30,31] which is characteristically labeled with PNA.[30–32] We found that every *Nrl*$^{-/-}$ photoreceptor has a sheathlike matrix structure that binds PNA (Figs. 3A–3C). Details of this sheath other than its overall length were very similar to that of the WT mouse cone, including the apparent termination of the sheath at the OLM and the RPE apical surface (Figs. 3D–3F), except in cases where the ONL forms a rosette.

The presence of rosettes in the *Nrl*$^{-/-}$ retina, in which the outermost nuclei of the ONL are displaced far from the RPE apical surface in a basketlike depression,[5] provided an opportunity to examine further the nature of the *Nrl*$^{-/-}$ photoreceptor sheath material (Fig. 4). Despite their displacement from the RPE, each of the photoreceptors forming the rim of the rosette has an associated sheath, and the sheathlike material extends into the interior of the rosette, which appears to be filled with the UV-cone pigment membranes. These observations reveal that the sheath material is still produced when the photoreceptors are no

longer in proximity to the RPE and also suggests that at such a distance from the RPE, neither the sheath nor the cone outer segment membranes can be properly degraded.

Quantification of the Principal Photoreceptor Proteins in the *Nrl*$^{-/-}$ Retina

In WT retina, the three most abundant proteins are the rod phototransduction proteins rhodopsin, transducin, and arrestin, and we undertook to determine the amounts of the homologous cone proteins in the *Nrl*$^{-/-}$ retina. Quantitative immunoblot analysis (Figs. 5A, 5B) revealed the quantity of the MUV pigment to be 81 ± 9 picomoles/eye (mean ± SEM, n = 7 eyes from four different 5-week-old mice). Using the same extraction procedure, but bleaching difference spectroscopy for quantitation, we extracted 520 ± 40 picomoles/eye rhodopsin from 4 age-matched WT controls. Immunoblot analysis also revealed the amount of cone transducin ($G_t\alpha 2$) to be 14 times and cone arrestin (mCarr) to be 12 times more abundant in the *Nrl*$^{-/-}$ retina than in the WT retina (Fig. 5C).

The relative abundance of these three proteins of the cone phototransduction cascade are roughly consistent with expectations based on the relative number of rod and cones in the WT retina, our estimate of the number of photoreceptors in the *Nrl*$^{-/-}$ retina, and the sizes of the outer segments, and the hypothesis that *Nrl*$^{-/-}$ photoreceptors are cones. For MUV: given (1) that there are ~60% as many photoreceptors in the *Nrl*$^{-/-}$ retina as rods in the WT mouse, (2) that the OS volume of the *Nrl*$^{-/-}$ photoreceptor is ~one fourth that of the WT rod (Table 1), and (3) that the membranes of the *Nrl*$^{-/-}$ photoreceptor OS contain MUV at the same density as the rod discs, we would then expect, relative to 520 picomoles rhodopsin recovered from the WT eye, to recover ~520 × 0.6 × 0.25 = 78 picomoles MUV, compared with the 80 picomoles measured. For Gnat2: given (1) that cones constitute 3% of the photoreceptors of the WT retina; (2) that there are ~60% as many photoreceptors in the *Nrl*$^{-/-}$ retina as rods in the WT, and thus 0.6 × 30 = 18-fold as many cones in the *Nrl*$^{-/-}$ as in the WT; and (3) that Gnat2 resides in the OS, whose volume in the *Nrl*$^{-/-}$ is 60% that of the WT cone (Table 1), then the abundance of Gnat2 in the *Nrl*$^{-/-}$ retina relative to that of the WT is expected to be 1:18 × 0.6 = 1:11, compared with the observed ratio 1:14. For mCarr: with the same given as for Gnat2, except assuming mCarr is distributed throughout the cone cytoplasm,[33,34] the relative abundance in *Nrl*$^{-/-}$ relative to WT is predicted to be 1:18, compared with the 1:12 observed.

Relative Magnitudes of the Massed Photoreceptor Responses of *Nrl*$^{-/-}$ and WT Mice In Vivo

The saturated a-wave amplitude is directly proportional to the instantaneous magnitude of the circulating current of the photoreceptors (reviewed in Ref. 6). In the WT mouse >95% of the a-wave originates in rod-driven current, and the saturating amplitude of the cone a-wave is only 10 to 15 μV, compared with a saturating rod a-wave amplitude in age-matched control eyes of 350 to 550 μV.[15] The a-wave is readily recordable from the *Nrl*$^{-/-}$ retina (Fig. 6A): its saturating amplitude in 4- to 6-week-old mice was a_{max} = 120 ± 4 μV (mean ± SEM, n = 33), as contrasted with a_{max} = 550 ± 88 μV (n = 8) for that of the rod a-wave of age-matched WT control mice also measured with the reference electrode in the mouth (Fig. 6B). From these observations it is thus estimated that the current density produced by the *Nrl*$^{-/-}$ photoreceptors is 120/550 = 0.22 of that produced by rods in the WT retina. If, in the

dark adapted eye, the density of open cGMP-activated channels in rods and $Nrl^{-/-}$ photoreceptors per unit length of the OS is the same (cf. Table 1), the ratio of the saturating a-wave amplitudes is predicted to be 0.6 × (7/24) = 0.18, assuming (as mentioned earlier) 60% as many photoreceptors in the $Nrl^{-/-}$ as in the WT retina and OS lengths of 7 and 24 μm, respectively. If the ratio of cGMP channels per unit length of OS, and the concentration of pigment in the disc membranes is conserved between rod and $Nrl^{-/-}$ photoreceptors, the ratio of the saturating a-wave amplitudes would also be expected to be close to the mole ratio of rhodopsin to MUV extracted per eye. Given the 17% greater diameter of the rod OS relative to the $Nrl^{-/-}$ OS (Table 1), the predicted pigment mole ratio is $0.22 \times (1/1.17)^2 = 0.16$; the measured mole ratio is 80 picomoles/520 picomoles = 0.15. The general agreement between these predictions and measurements indicates that the major phototransduction proteins are present in comparable amounts in WT rods and $Nrl^{-/-}$ photoreceptors.

Other Factors Potentially Contributing to the Relatively Low Saturating Amplitude of the a-Wave

The saturating amplitude of the a-wave, a_{max}, is proportional to the massed circulating current of the photoreceptors,[6,35,36] but the proportionality constant depends on several other factors, including the number of photoreceptors and the thicknesses and resistivities of the retinal layers.[37] The question may be raised whether the altered structure of the photoreceptor layer in the $Nrl^{-/-}$ retina—as opposed to decreased magnitude of the massed circulating current of the photoreceptors—contributes to the lower value of a_{max} of the $Nrl^{-/-}$ relative to that generated by the rods of the WT retina. A definitive answer to this question requires a complete layer resistivity and current source–sink analysis.[35,38] We addressed this question with a simplification of a previously published source–sink analysis,[6] which gives an analytical approximation of the relationship between the circulating current and transphotoreceptor layer potential. We assumed no change in the nonphotoreceptor layers (e.g., RPE), so that the difference in a_{max} between $Nrl^{-/-}$ and WT depends only on the transreceptor layer potential. As the outer segment layer contributes little to the transreceptor layer potential in WT due to its relatively low resistivity,[6,35] the main factor other than the massed circulating current that determines the transreceptor layer potential is the resistance of the ONL. Because the ONL thickness of the $Nrl^{-/-}$ retina is very close to that of the WT (Fig. 2 in Ref. 5), the only factor at issue is the resistivity of the ONL, and indeed, the published analysis (see equation AI.6 in Ref. 6) shows the transreceptor layer potential to be effectively proportional to this resistivity. This resistivity may be decreased in the $Nrl^{-/-}$ retina relative to WT, due to its somewhat fewer (but larger) ONL nuclei and stout myoids (Fig. 2), but we doubt that the resistivity could be 20% lower than in WT retina. We conclude that the predominant factor in the decreased a_{max} of $Nrl^{-/-}$ relative to WT is the lowered massed photoreceptor circulating current.

Amplification of Phototransduction in $Nrl^{-/-}$ Photoreceptors

To assess phototransduction in $Nrl^{-/-}$ photoreceptors, we analyzed families of a-waves with a model of the phototransduction cascade[18,19] to extract A, the amplification constant (Figs. 6C, 6D). For the $Nrl^{-/-}$ a-wave activated by 360 nm stimulation, $A = 4.0 \pm 0.3\ s^{-2}$ (mean ± SEM, $n = 13$). Measured under the same conditions in age-matched WT control eyes stimulated with 500 nm flashes, $A = 8.2 \pm 0.5\ s^{-2}$ (mean ± SEM, $n = 8$), approximately two

times higher than that of the $Nrl^{-/-}$ a-wave. It bears mentioning that the determination of A requires estimation of the number of photoisomerizations produced per flash in the photoreceptor, and that we have made the assumption that funneling by the $Nrl^{-/-}$ photoreceptor inner segment increases the cell's light collection approximately fourfold. Were the adjustment for light funneling not made, the estimated amplification constant of the $Nrl^{-/-}$ photoreceptor would be four times higher—that is, $A = 16\ s^{-2}$—substantially higher than that of rods measured under the same conditions.

Activation of *Nrl*$^{-/-}$ Photoreceptors by UV- and M-Cone Pigments

By determining the dependence of the activation phase of the a-wave of the response on the wavelength of the stimulating flash, we measured the spectral sensitivity of the $Nrl^{-/-}$ photoreceptor response: sensitivity peaked at ~360 nm, and declined at higher wavelengths (Fig. 6E). However, sensitivity did not decline as steeply at longer wavelengths as predicted for a single pigment with $\lambda_{max} = 360$ nm (Fig. 6E, dashed line), but rather exhibited a secondary mode around 510 nm. This deviation from a single template can be fitted by assuming that light captured by the mouse M-cone pigment ($\lambda_{max} = 508$ nm[39]) drives the a-wave with a sensitivity approximately one tenth that of the UV-cone pigment.[40] The absence of rhodopsin expression and high levels of the M-cone transcripts in the $Nrl^{-/-}$ retina[5] establishes that the midwave sensitivity of the a-wave arises from light captured by the M-cone pigment.

Decline in the Saturating a-Wave Amplitude of the *Nrl*$^{-/-}$ Retina with Age

We have focused our investigations on the $Nrl^{-/-}$ photoreceptors of 4- to 6-week-old mice. The reason for restricting attention to animals in this age group is that the saturating amplitude (a_{max}) of the a-wave is stable in animals of this age, but declines thereafter (Fig. 6F). Thus, a_{max} for animals of age <42 days was ~120 μV, but by 80 days had declined to <60 μV ($P < 10^{-9}$).

Inactivation of Phototransduction in *Nrl*$^{-/-}$ Photoreceptors

Cone photoreceptor cells generally have faster time to peak and recovery kinetics than their rod counterparts in a given species. We applied the paired-flash ERG method to the a-wave to recover the complete time course of the massed photocur-rent response to UV flashes of the $Nrl^{-/-}$ retina in vivo (Fig. 7). The response to a flash that suppressed approximately 50% of the circulating current had a time to peak of ~50 ms (Figs. 7A, 7B). Likewise, the time to peak of the response to a flash that suppressed approximately 25% was <50 ms, whereas the responses to a UV flash that completely suppressed the circulating current recovered in a biphasic manner, with a rapid initial recovery followed by a much slower tail phase (Fig. 7C).

Summary of Features of *Nrl*$^{-/-}$ Photoreceptors

Table 1 summarizes the various ultrastructural, histochemical, molecular, and physiological characteristics of $Nrl^{-/-}$ photo-receptors, and compares these with the comparable features of WT mouse rods and (when possible) cones. Although $Nrl^{-/-}$ photoreceptors are not

identical to WT cones in their properties, they are clearly highly distinct from rods and can unequivocally be classified as a species of cones.

Discussion

Proper Classification of *Nrl*$^{-/-}$ Photoreceptors

In the absence of Nrl expression, rod photoreceptors do not develop and most rod-specific genes are not expressed.[5,9] The central question posed in this investigation was whether the photoreceptors of the *Nrl*$^{-/-}$ mouse are properly classified as cones, or whether they represent a distinct species of photo-receptors, perhaps intermediate between cones and rods. We addressed this question with structural (Fig. 1), ultrastructural (Fig. 2), histochemical (Fig. 3), molecular (Fig. 5), and electro-physiological (Figs. 6, 7) analyses. Our results show unequivocally that *Nrl*$^{-/-}$ photoreceptors are cone-like in their features (Table 1) and hence can properly be identified as cones. Nonetheless, *Nrl*$^{-/-}$ photoreceptor outer segments are shorter than those of WT cones, exhibit disorder, appear to deteriorate (Fig. 6F), and express "rod" arrestin.[5] Thus, they are not identical with normal WT mouse cones.

Phototransduction in *Nrl*$^{-/-}$ Photoreceptors

Key molecules of the cone phototransduction cascade—MUV, cone transducin, and cone arrestin—are present in amounts per cell comparable to those of the homologous transduction proteins that have been measured in the rods and amounts expected to be present in WT cones (Fig. 5). The photocurrent response of *Nrl*$^{-/-}$ photoreceptors, as manifest in the ERG a-wave, is driven largely by the mouse S(UV)-cone pigment (Fig. 6E), has an estimated amplification constant $A = 4.0\ s^{-2}$, comparable but reliably lower than that of WT rods ($A = 8.3\ s^{-2}$), and has a time-to-peak of the dim-flash response in vivo of 50 ms or less (Fig. 7). These latter properties establish that the proteins of the cone phototransduction cascade in *Nrl*$^{-/-}$ photoreceptors drive the photoresponse with high efficiency and cone-like recovery kinetics. Of special note is the brief time-to-peak of the dim-flash response, which is much shorter than that of rods (~140 ms) assayed in a similar paired flash paradigm,[41] and comparable to that previously reported in single-cell recordings from S-cones in some other mammals.[42,43] Further evidence of healthy phototransduction in *Nrl*$^{-/-}$ photoreceptors is provided by single-cell recordings.[27]

Utility of the *Nrl*$^{-/-}$ Mouse for the Investigation of Cone Function and Disease

In addition to its demonstrated utility in the investigation of photoreceptor differentiation,[3,5] the *Nrl*$^{-/-}$ retina should facilitate molecular studies of cone function. The *Nrl*$^{-/-}$ mouse has been used to establish for the first time the G-protein receptor kinase–dependent phosphorylation of MUV pigment, and the phosphorylation-dependent binding of cone arrestin (mCarr).[9] These molecular functions have long been investigated in rods, but have eluded study in mammalian cones. The *Nrl*$^{-/-}$ retina has been used to establish a remarkable plasticity of synaptic connections between photoreceptors and second-order neurons.[44]

Our work reveals new ways in which the *Nrl*$^{-/-}$ retina will be valuable in the investigation of cones. For example, each *Nrl*$^{-/-}$ photoreceptor, like WT mouse cones, has associated with it a PNA-stained sheath (Fig. 3C). In WT mice and other species, the PNA-stained sheath is

tethered to the RPE and surrounds both the outer segment and the inner segment as far as the outer limiting membrane.[30,32,45] Even *Nrl*$^{-/-}$ photoreceptors far removed from the RPE cell apical surface in rosettes possess such sheaths (Fig. 4). This observation supports the interesting hypothesis that the sheath is secreted by the cones themselves. Microarray analysis has provided a catalog of the genes with increased expression in the *Nrl*$^{-/-}$ relative to WT.[3] Such gene profiling may now help in uncovering the genes involved in the generation of the cone sheath.

The *Nrl*$^{-/-}$ retina also allows the power of mouse molecular genetics to be used in the investigation of the functional properties of single mouse cone photoreceptor cells, a strategy that has been so successful in the investigation of rod photo-transduction.[46–51]

The Nature of the Rosettes in the ONL

Nuclei in the ONL of the *Nrl*$^{-/-}$ retina sometimes form rosettes, and the presence of MUV and PNA-stained material indicates that these nuclei are those of mislocated cones (Fig. 4). Cone nuclei in WT retina normally localize in the outermost layer of the ONL (Fig. 1 in Ref. 28), and hence we hypothesize that the larger number of cones in the *Nrl*$^{-/-}$ retina leads to the formation of an overpopulated layer or surface that buckles inward, like the infoldings of the cerebral cortex. The cells in the rosettes appear to deteriorate, most likely because their detachment from the RPE results in the failure of OS membrane and matrix sheath turnover (Fig. 4).

Disorder and Deterioration in the Photoreceptor Layer of the *Nrl*$^{-/-}$

Photoreceptor function is healthy and stable in the *Nrl*$^{-/-}$ retina during the period 4 to 6 weeks but deteriorates subsequently, as revealed by a decline in the saturating amplitude of the a-wave (Fig. 6F), which reflects a declining massed circulating current of the photoreceptor cells. This deterioration, along with the relative disorder in the photoreceptor layer (Fig. 3 in Ref. 5), calls for caution but also provides an opportunity for investigating the nature of the disorder and degeneration. Three non–mutually exclusive hypotheses bear mentioning, all of which involve the absence of rods: (1) In the WT retina the tip of the cone OS is removed from the RPE apical surface by 10 to 15 μm, but connected to the RPE via its matrix sheath (Figs. 3C, 3F; Refs. 28, 45). In contrast, in the *Nrl*$^{-/-}$ the absence of the rods places the cone OS tips in apposition to the RPE (Figs. 2, 3). As a consequence normal interactions between the RPE and the cone OSs may be perturbed, potentially affecting critical processes such as the phagocytosis of disc membranes. (2) The photoreceptor circulating current produces a very high demand for oxygen supplied by the choroidal circulation.[52,53] The average saturating amplitude of the a-wave of the *Nrl*$^{-/-}$ retina, a_{max} = 120 μV (Fig. 6), is about one fourth that of the WT. Therefore, the average circulating current density and oxygen demand in *Nrl*$^{-/-}$ should be approximately one fourth that of the WT, which must use four times more energy to “bail out” the Na^{2+} that flows into the OS through the cGMP-gated channels of rods in the dark adapted retina. Thus, oxygen tension in the photoreceptor layer of the *Nrl*$^{-/-}$ retina should be higher than in WT, as in the P23H rat,[54] and such hyperoxia can be toxic to photoreceptors.[55] (3) It has been reported that rods express a factor that enhances the survival of cones in certain retinal degenerations.[56] Such a factor should be absent in the *Nrl*$^{-/-}$ retina.

Mutations or Deletions in *Nr2e3*, Enhanced Short-Wave Cone Syndrome, and *Nrl*$^{-/-}$

Our observations of a photoreceptor degeneration in the *Nrl*$^{-/-}$ retina as measured by the age-dependent decrease in saturated ERG a-wave amplitude (Fig. 6F) is consistent with the human hereditary retinal degenerations caused by missense mutations in *NRL* as well as *NR2E3*, a transcription factor downstream of *NRL*.[5] Humans with mutations in *NRL* have autosomal dominant retinitis pigmentosa, and electroretinography reveals a severe loss of both rod and cone function.[4,57] It is tempting then to compare the S-cone function of *Nrl*$^{-/-}$ mouse retina with patients with enhanced short-wave cone syndrome (ESCS) who have missense mutations in the *NR2E3* gene, but have less severe degeneration of cone function and an increased ratio of S-cones to L/M-cones (i.e., ESCS).[58–61] However, there are important differences in the consequences of *NR2E3* defects and deletion of *Nrl* in mice. Deletion or mutations of *NR2E3* or *Nr2e3* result in abnormal rods that degenerate with time,[59,62] whereas deletion of *Nrl* results in a retina with no morphologically distinct or functional rods (Figs. 1, 2, 3 in Ref. 5). In addition, cone-derived ERGs, psychophysical tests and postmortem immunohistochemistry in patients with ESCS reveal the function of their S-cones to be more severely compromised than that of the cones of young *Nrl*$^{-/-}$ mice.[61] Photoreceptor responses (measured with the paired-flash method) of human ESCS patients' S-cones were found to recover much more slowly than those of L/M-cones, and postmortem immunohistochemistry revealed undetectable GRK1 expression.[61] In contrast, all *Nrl*$^{-/-}$ photoreceptors express Grk1,[9] and single-cell recordings,[27] as well as the paired flash a-wave data presented herein (Fig. 7), show that the time to peak of the dim-flash response and the recovery kinetics of saturated responses of *Nrl*$^{-/-}$ photoreceptors are much faster than the comparable features of WT rods, suggesting healthy cone function.

Arrestin and Grk1 Expression in *Nrl*$^{-/-}$ Photoreceptors and the Nature of Cones

Based on multiple criteria, we have concluded that *Nrl*$^{-/-}$ photoreceptors are cones (Table 1). Nonetheless, our battery is not exhaustive and *Nrl*$^{-/-}$ cones and WT cones should be compared on a longer list of molecular criteria to assess their similarities to each other and their differences from rods. Two proteins often thought to be rod specific, Grk1 (rhodopsin kinase) and arrestin, bear mentioning in this context. Grk1 is expressed not only in rods, but also in all cones of most mammalian retinas examined so far,[63,64] including those of primates.[61,65,66] Moreover, in the mouse, Grk1 is necessary for normal inactivation of cone phototransduction.[16] Arrestin is expressed not only in rods, but also in RPE cells[67] and in developing cones[68] and may be expressed in WT mouse cones (cf. Table 1). Hence, the classification of photoreceptors cannot be made on the basis of the expression of individual proteins.

Acknowledgments

The authors thank Cheryl Craft and Xuemei Zhu (Doheny Eye Institute and Dept. of Ophthalmology, University of Southern California) for providing antibodies against MUV protein, and Barry Knox and Kunnel Babu (SUNY Upstate Medical Center, Syracuse, NY) for recombinant MUV.

Supported National Eye Institute EY-02660; EY-11115, EY13408; The Foundation Fighting Blindness; and Research to Prevent Blindness Foundation.

References

1. Swaroop A, Xu JZ, Pawar H, et al. A conserved retina-specific gene encodes a basic motif/leucine zipper domain. Proc Natl Acad Sci USA. 1992; 89:266–270. [PubMed: 1729696]
2. Swain PK, Hicks D, Mears AJ, et al. Multiple phosphorylated iso-forms of NRL are expressed in rod photoreceptors. J Biol Chem. 2001; 276:36824–36830. [PubMed: 11477108]
3. Yoshida S, Mears AJ, Friedman JS, et al. Expression profiling of the developing and mature $Nrl^{-/-}$ mouse retina: identification of retinal disease candidates and transcriptional regulatory targets of Nrl. Hum Mol Genet. 2004; 13:1487–1503. [PubMed: 15163632]
4. Bessant DA, Payne AM, Mitton KP, et al. A mutation in NRL is associated with autosomal dominant retinitis pigmentosa. Nat Genet. 1999; 21:355–356. [PubMed: 10192380]
5. Mears AJ, Kondo M, Swain PK, et al. Nrl is required for rod photoreceptor development. Nat Genet. 2001; 29:447–452. [PubMed: 11694879]
6. Pugh, EN., Jr; Falsini, B.; Lyubarksy, AL. Photostasis and Related Phenomena. Plenum Press; New York: 1998. The origin of the major rodand cone-driven components of the rodent electroretinogram and the effect of age and light-rearing history on the magnitude of these components.; p. 98-128.
7. Arikawa K, Molday LL, Molday RS, Williams DS. Localization of peripherin/rds in the disk membranes of cone and rod photoreceptors: relationship to disk membrane morphogenesis and retinal degeneration. J Cell Biol. 1992; 116:659–667. [PubMed: 1730772]
8. Gibbs D, Azarian SA, Lillo C, et al. Role of myosin VIIa and Rab27a in the motility and localization of RPE melanosomes. J Cell Sci. 2004; 117:6473–6483. [PubMed: 15572405]
9. Zhu X, Brown B, Li A, et al. GRK1-dependent phosphorylation of S and M opsins and their binding to cone arrestin during cone phototransduction in the mouse retina. J Neurosci. 2003; 23:6152–6160. [PubMed: 12853434]
10. Van Hooser JP, Garwin GG, Saari JC. Analysis of visual cycle in normal and transgenic mice. Methods Enzymol. 2000; 316:565–575. [PubMed: 10800702]
11. Vought BW, Dukkipatti A, Max M, Knox BE, Birge RR. Photochemistry of the primary event in short-wavelength visual opsins at low temperature. Biochemistry. 1999; 38:11287–11297. [PubMed: 10471278]
12. Starace DM, Knox BE. Cloning and expression of a Xenopus short wavelength cone pigment. Exp Eye Res. 1998; 67:209–220. [PubMed: 9733587]
13. Gill SC, von Hippel PH. Calculation of protein extinction coefficients from amino acid sequence data. Anal Biochem. 1989; 182:319–326. [PubMed: 2610349]
14. Dukkipati A, Kusnetzow A, Babu KR, et al. Phototransduction by vertebrate ultraviolet visual pigments: protonation of the retinylidene Schiff base following photobleaching. Biochemistry. 2002; 41:9842–9851. [PubMed: 12146950]
15. Lyubarsky AL, Falsini B, Pennesi ME, Valentini P, Pugh EN Jr. UV-and midwave-sensitive cone-driven retinal responses of the mouse: a possible phenotype for coexpression of cone photopigments. J Neurosci. 1999; 19:442–455. [PubMed: 9870972]
16. Lyubarsky AL, Chen C, Simon MI, Pugh EN Jr. Mice lacking G-protein receptor kinase 1 have profoundly slowed recovery of cone-driven retinal responses. J Neurosci. 2000; 20:2209–2217. [PubMed: 10704496]
17. Lyubarsky AL, Pugh EN Jr. Recovery phase of the murine rod photoresponse reconstructed from electroretinographic recordings. J Neurosci. 1996; 16:563–571. [PubMed: 8551340]
18. Lamb TD, Pugh EN Jr. A quantitative account of the activation steps involved in phototransduction in amphibian photoreceptors. J Physiol. 1992; 449:719–758. [PubMed: 1326052]
19. Pugh EN Jr, Lamb TD. Amplification and kinetics of the activation steps in phototransduction. Biochim Biophys Acta. 1993; 1141:111–149. [PubMed: 8382952]
20. Leskov IB, Klenchin VA, Handy JW, et al. The gain of rod phototransduction: reconciliation of biochemical and electrophysiological measurements. Neuron. 2000; 27:525–537. [PubMed: 11055435]

21. Pugh, EN., Jr; Lamb, TD. Phototransduction in vertebrate rods and cones: molecular mechanisms of amplification, recovery and light adaptation.. In: Stavenga, DG.; DeGrip, WJ.; Pugh, EN., Jr., editors. Molecular Mechanisms in Visual Transduction. Elsevier; New York: 2000. p. 183-255.
22. Smith NP, Lamb TD. The a-wave of the human electroretinogram recorded with a minimally invasive technique. Vision Res. 1997; 37:2943–2952. [PubMed: 9425511]
23. Lyubarsky AL, Daniele LL, Pugh EN Jr. From candelas to photoisomerizations in the mouse eye by rhodopsin bleaching in situ and the light-rearing dependence of the major components of the mouse ERG. Vision Res. 2004; 44:3235–3251. [PubMed: 15535992]
24. Enoch, JM.; Tobey, F. Waveguide properties of retinal receptors: techniques and observations.. In: Enoch, JM.; Tobey, FL., Jr., editors. Vertebrate Photoreceptor Optics. Springer; New York: 1981. p. 169-218.
25. Horowitz, T. Theoretical considerations of the retinal receptor as a waveguide.. In: Enoch, JM.; Tobey, FL., Jr., editors. Vertebrate Photoreceptor Optics. Springer; New York: 1981. p. 219-300.
26. Baylor DA, Fettiplace R. Transmission from photoreceptors to ganglion cells in turtle retina. J Physiol. 1977; 271:391–424. [PubMed: 200736]
27. Nikonov SS, Daniele LL, Zhu X, Craft CM, Swaroop A, Pugh EN Jr. Photoreceptors of Nrl mice coexpress functional S- and M-cone opsins having distinct inactivation mechanisms. J Gen Physiol. 2005; 125:287–304. [PubMed: 15738050]
28. Carter-Dawson LD, LaVail MM. Rods and cones in the mouse retina. I. Structural analysis using light and electron microscopy. J Comp Neurol. 1979; 188:245–262. [PubMed: 500858]
29. Steinberg RH, Fisher SK, Anderson DH. Disc morphogenesis in vertebrate photoreceptors. J Comp Neurol. 1980; 190:501–508. [PubMed: 6771304]
30. Johnson LV, Hageman GS, Blanks JC. Interphotoreceptor matrix domains ensheathe vertebrate cone photoreceptor cells. Invest Ophthalmol Vis Sci. 1986; 27:129–135. [PubMed: 3080382]
31. Hageman GS, Johnson LV. Structure, composition and function of the retinal interphotoreceptor matrix. Prog Retin Eye Res. 1991; 10:207–249.
32. Blanks JC, Hageman GS, Johnson LV, Spee C. Ultrastructural visualization of primate cone photoreceptor matrix sheaths. J Comp Neurol. 1988; 270:288–300. [PubMed: 3379160]
33. Zhang H, Cuenca N, Ivanova T, et al. Identification and light-dependent translocation of a cone-specific antigen, cone arrestin, recognized by monoclonal antibody 7G6. Invest Ophthalmol Vis Sci. 2003; 44:2858–2867. [PubMed: 12824223]
34. Zhang H, Huang W, Zhang H, et al. Light-dependent redistribution of visual arrestins and transducin subunits in mice with defective phototransduction. Mol Vis. 2003; 9:231–237. [PubMed: 12802257]
35. Hagins WA, Penn RD, Yoshikami S. Dark current and photocurrent in retinal rods. Biophys J. 1970; 10:380–412. [PubMed: 5439318]
36. Penn RD, Hagins WA. Kinetics of the photocurrent of retinal rods. Biophys J. 1972; 12:1073–1094. [PubMed: 5044581]
37. Rodieck, RW. The Vertebrate Retina: Principles of Structure and Function. WH Freeman, Co.; San Francisco: 1973.
38. Karwoski CJ, Frambach DA, Proenza LM. Laminar profile of resistivity in frog retina. J Neurophysiol. 1985; 54:1607–1619. [PubMed: 3878863]
39. Sun H, Macke JP, Nathans J. Mechanisms of spectral tuning in the mouse green cone pigment. Proc Natl Acad Sci USA. 1997; 94:8860–8865. [PubMed: 9238068]
40. Yokoyama S, Radlwimmer FB, Kawamura S. Regeneration of ultra-violet pigments of vertebrates. FEBS Lett. 1998; 423:155–158. [PubMed: 9512349]
41. Hetling JR, Pepperberg DR. Sensitivity and kinetics of mouse rod flash responses determined in vivo from paired-flash electroretino-grams. J Physiol. 1999; 516:593–609. [PubMed: 10087356]
42. Schnapf JL, Nunn BJ, Meister M, Baylor DA. Visual transduction in cones of the monkey Macaca fascicularis. J Physiol. 1990; 427:681–713. [PubMed: 2100987]
43. Kraft TW. Photocurrents of cone photoreceptors of the golden-mantled ground squirrel. J Physiol. 1988; 404:199–213. [PubMed: 3253431]

44. Strettoi E, Mears AJ, Swaroop A. Recruitment of the rod pathway by cones in the absence of rods. J Neurosci. 2004; 24:7576–7582. [PubMed: 15329405]
45. Hageman GS, Marmor MF, Yao XY, Johnson LV. The interphoto-receptor matrix mediates primate retinal adhesion. Arch Ophthalmol. 1995; 113:655–660. [PubMed: 7748138]
46. Chen CK, Burns ME, Spencer M, et al. Abnormal photoresponses and light-induced apoptosis in rods lacking rhodopsin kinase. Proc Natl Acad Sci USA. 1999; 96:3718–3722. [PubMed: 10097103]
47. Chen CK, Burns ME, He W, et al. Slowed recovery of rod photo-response in mice lacking the GTPase accelerating protein RGS9–1. Nature. 2000; 403:557–560. [PubMed: 10676965]
48. Chen J, Makino CL, Peachey NS, Baylor DA, Simon MI. Mechanisms of rhodopsin inactivation in vivo as revealed by a COOH-terminal truncation mutant. Science. 1995; 267:374–377. [PubMed: 7824934]
49. Mendez A, Burns ME, Sokal I, et al. Role of guanylate cyclase-activating proteins (GCAPs) in setting the flash sensitivity of rod photoreceptors. Proc Natl Acad Sci USA. 2001; 98:9948–9953. [PubMed: 11493703]
50. Mendez A, Burns ME, Roca A, et al. Rapid and reproducible deactivation of rhodopsin requires multiple phosphorylation sites. Neuron. 2000; 28:153–164. [PubMed: 11086991]
51. Xu J, Dodd RL, Makino CL, et al. Prolonged photoresponses in transgenic mouse rods lacking arrestin. Nature. 1997; 389:505–509. [PubMed: 9333241]
52. Wangsa-Wirawan ND, Linsenmeier RA. Retinal oxygen: fundamental and clinical aspects. Arch Ophthalmol. 2003; 121:547–557. [PubMed: 12695252]
53. Shonat RD, Kight AC. Oxygen tension imaging in the mouse retina. Ann Biomed Eng. 2003; 31:1084–1096. [PubMed: 14582611]
54. Yu DY, Cringle S, Valter K, et al. Photoreceptor death, trophic factor expression, retinal oxygen status, and photoreceptor function in the P23H rat. Invest Ophthalmol Vis Sci. 2004; 45:2013–2019. [PubMed: 15161870]
55. Yamada H, Yamada E, Ando A, et al. Fibroblast growth factor-2 decreases hyperoxia-induced photoreceptor cell death in mice. Am J Pathol. 2001; 159:1113–1120. [PubMed: 11549604]
56. Leveillard T, Mohand-Said S, Lorentz O, et al. Identification and characterization of rod-derived cone viability factor. Nat Genet. 2004; 36:755–759. [PubMed: 15220920]
57. Martinez-Gimeno M, Maseras M, Baiget M, et al. Mutations P51U and G122E in retinal transcription factor NRL associated with autosomal dominant and sporadic retinitis pigmentosa. Hum Mutat. 2001; 17:520. [PubMed: 11385710]
58. Hood DC, Cideciyan AV, Roman AJ, Jacobson SG. Enhanced S cone syndrome: evidence for an abnormally large number of S cones. Vision Res. 1995; 35:1473–1481. [PubMed: 7645276]
59. Haider NB, Jacobson SG, Cideciyan AV, et al. Mutation of a nuclear receptor gene, NR2E3, causes enhanced S cone syndrome, a disorder of retinal cell fate. Nat Genet. 2000; 24:127–131. [PubMed: 10655056]
60. Milam AH, Rose L, Cideciyan AV, et al. The nuclear receptor NR2E3 plays a role in human retinal photoreceptor differentiation and degeneration. Proc Natl Acad Sci USA. 2002; 99:473–478. [PubMed: 11773633]
61. Cideciyan AV, Jacobson SG, Gupta N, et al. Cone deactivation kinetics and GRK1/GRK7 expression in enhanced S cone syndrome caused by mutations in *NR2E3*. Invest Ophthalmol Vis Sci. 2003; 44:1268–1274. [PubMed: 12601058]
62. Akhmedov NB, Piriev NI, Chang B, et al. A deletion in a photoreceptor-specific nuclear receptor mRNA causes retinal degeneration in the rd7 mouse. Proc Natl Acad Sci USA. 2000; 97:5551–5556. [PubMed: 10805811]
63. Chen CK, Zhang K, Church-Kopish J, et al. Characterization of human GRK7 as a potential cone opsin kinase. Mol Vis. 2001; 7:305–313. [PubMed: 11754336]
64. Weiss ER, Ducceschi MH, Horner TJ, et al. Species-specific differences in expression of G-protein-coupled receptor kinase (GRK) 7 and GRK1 in mammalian cone photoreceptor cells: implications for cone cell phototransduction. J Neurosci. 2001; 21:9175–9184. [PubMed: 11717351]

65. Sears S, Erickson A, Hendrickson A. The spatial and temporal expression of outer segment proteins during development of Macaca monkey cones. Invest Ophthalmol Vis Sci. 2000; 41:971–979. [PubMed: 10752930]

66. Cideciyan AV, Zhao X, Nielsen L, et al. Null mutation in the rhodopsin kinase gene slows recovery kinetics of rod and cone phototransduction in man. Proc Natl Acad Sci USA. 1998; 95:328–333. [PubMed: 9419375]

67. Nicolas C, Ghedira I, Stiemer R, et al. Identification of visual arrestin (S-antigen) in retinal pigmented epithelial cells. Curr Eye Res. 2000; 21:677–683. [PubMed: 11120555]

68. Long K, Philp N, Gery I, Aguirre G. S-antigen in a hereditary visual cell disease: immunocytochemical and immunological studies. Invest Ophthalmol Vis Sci. 1988; 29:1594–1607. [PubMed: 3182194]

69. Lamb TD. Photoreceptor spectral sensitivities: common shape in the long-wavelength region. Vision Res. 1995; 35:3083–3091. [PubMed: 8533344]

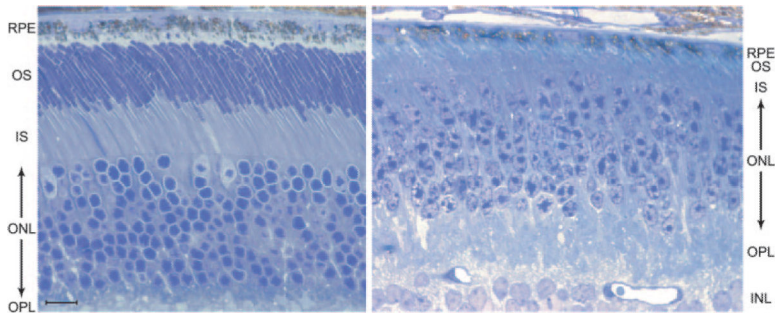

Figure 1.

Light micrograph of a semithin section of the RPE and photoreceptor layers of the retina of a 5-week-old *Nrl*$^{-/-}$ mouse (*right*) and age-matched WT mouse (*left*). Note the three cone nuclei (pale-staining nucleoplasm) in the outermost layer of the ONL of the WT retina. RPE, retinal pigment epithelium cell layer; OS, outer segment layer; IS, inner segment layer; ONL, outer nuclear layer; OPL, outer plexiform; INL, inner nuclear layer. Bar, 10 μm.

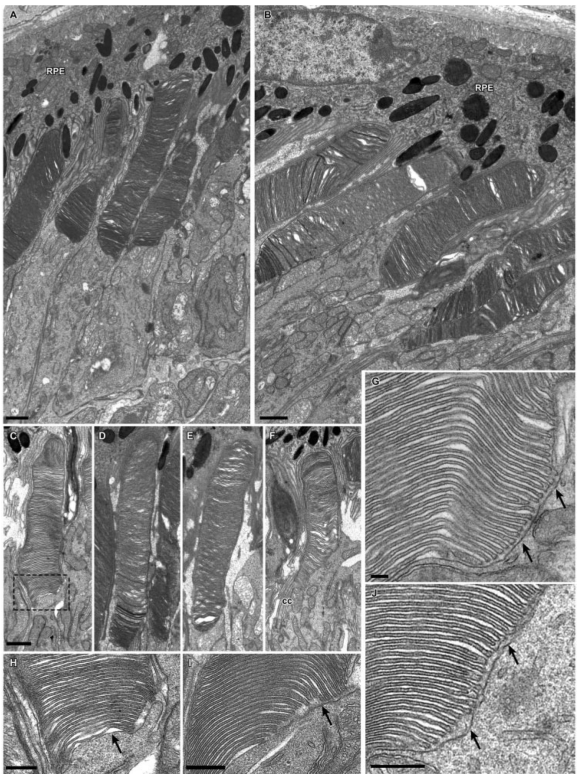

Figure 2.

Electron micrographs of photoreceptor cells from *Nrl*$^{-/-}$ retinas. (**A, B**) Groups of photoreceptor cells and adjacent RPE. (**C–F**) Examples of individual photoreceptor outer segments. Although less organized than normal outer segments, the disc membranes form a well-defined stack. Outlined area in (**C**) is shown at higher magnification in (**H**). (**G–J**) Higher magnification of the basal region of the outer segments from several photoreceptor cells. *Arrows*: inner segment membrane apposes the basal discs, which are open to the extracellular space; the region of open discs extends much further distally than observed for normal rod outer segments (cf. Ref. 28). RPE, retinal pigmented epithelium; CC, connecting cilium. Scale bars: (**A–F**) 1 μm; (**G–J**) 300 nm.

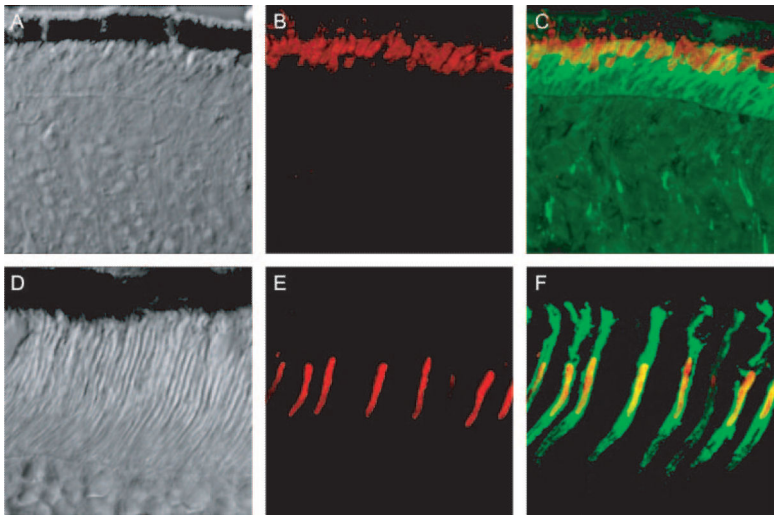

Figure 3.

(**A–C**) Images of a frozen section of *Nrl*$^{-/-}$ retina taken with differential interference contrast optics (**A**), with fluorescent immuno-staining of MUV, the mouse ultraviolet pigment (**B**, *red*), and with overlaid fluorescent immunostaining of MUV and PNA binding (*green*) (**C**). (**D–F**) Images of a frozen section of a WT retina stained and presented in the same format as in (**A–C**). Images were made with a confocal microscope and represent 50 × 50-μm regions of the two retinas.

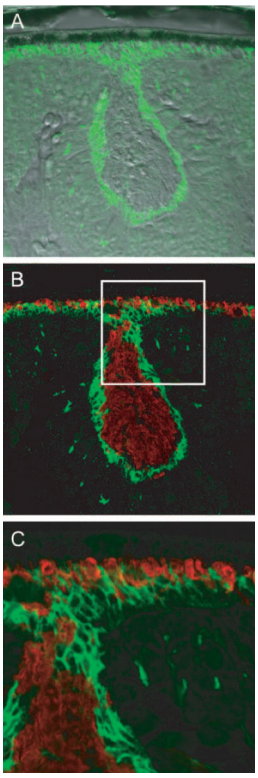

Figure 4.

Confocal images of a rosette in the ONL of the *Nrl*$^{-/-}$ retina. (**A**) Differential interference contrast image with overlaid image taken of PNA labeling (*green*). (**B**) Same section as in (**A**), but merging immunostaining of MUV (*red*) and PNA labeling. MUV is seen to fill the center portion of the rosette; the *white square* is 50 × 50 μm. (**C**) Magnified image of the portion of (**B**) highlighted by the *white square*, showing details of a portion of the rosette. Note how the PNA labeling of the border of the rosette merges with the PNA-stained inner segment layer of the cones that are in contact with the RPE.

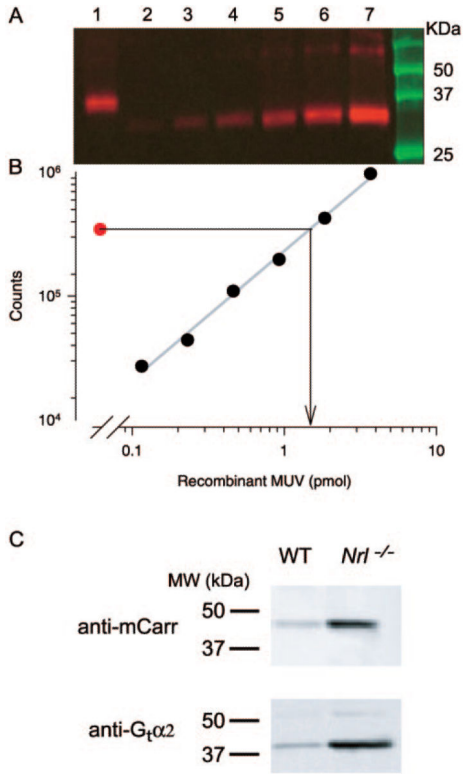

Figure 5.

Immunoblot analysis of cone phototransduction cascade molecules in the *Nrl*$^{-/-}$ retina. (**A**) Immunoblot of the mouse UV-cone pigment (MUV) of a 4-week-old *Nrl*$^{-/-}$ mouse: *lane 1*: 1% of the lysate of two *Nrl*$^{-/-}$ eyes; *lanes 2* to *7*: twofold incremented amounts of recombinant MUV; the latter runs at a slightly lower molecular mass because of mutations engineered to allow it to be purified with a commercial antibody.[12] (**B**) Plot of the blot densities in (**A**): each point (●) corresponds to the density of the MUV immunolabeling in the blot lane immediately above it in (**A**). The *symbol* corresponding to *lane 1* yields the estimate of the MUV mass loaded from the *Nrl*$^{-/-}$ eye, 1.6 picomoles (*arrow* projecting to abscissa). Because 1% of the lysate of two eyes was loaded in *lane 1*, the MUV per eye is thus estimated to be 80 picomoles. (**C**) Blots comparing extracts of *Nrl*$^{-/-}$ and WT mouse eyes for cone arrestin (mCarr) and the α-subunit of cone transducin ($G_t\alpha 2$): 25 μg of protein from eyes of animals of each genotype was loaded into adjacent lanes of the gel and immunolabeled. The blot densities of regions circumscribing the immunolabel were quantified, and the ratio of the densities for the blots of the WT and *Nrl*$^{-/-}$ lanes were determined. The ratios were 14:1 for the mCarr comparison and 11:1 for the $G_t\alpha 2$ comparison in the blots illustrated. Mean ratios (± SEM) were 12.3 ± 1.1 for mCarr (two blots, 11 comparisons of proteins from five *Nrl*$^{-/-}$ and two WT mice), and 14.1 ± 2.4 for $G_t\alpha 2$ (three blots, 21 comparisons).

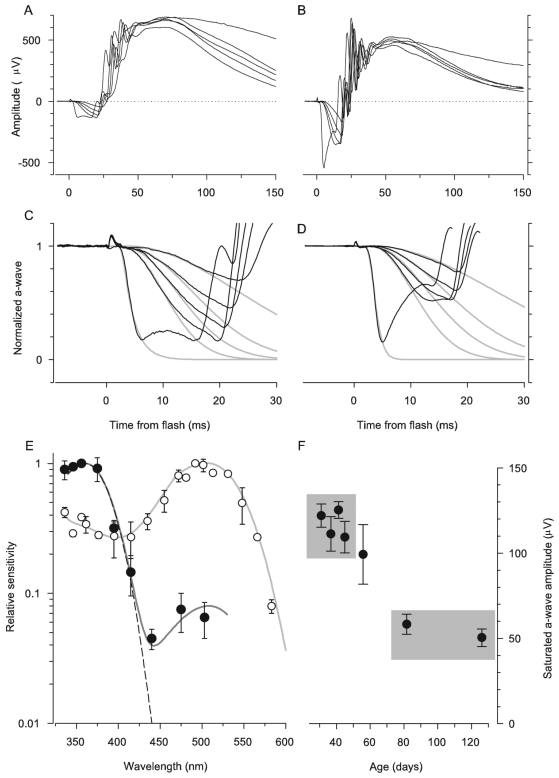

Figure 6.

Comparison of the properties of the ERG a-wave responses of $Nrl^{-/-}$ and WT mice. (**A**) ERGs of an $Nrl^{-/-}$ mouse obtained in response to a series of 360-nm flashes that produced a-waves. The flash intensities were 7,400, 21,000, 36,400, 68,000 in photons/μm^2 at the cornea. The most intense flash was an unattenuated white flash and saturated the a-wave amplitude. (**B**) ERGs of a WT mouse obtained in response to the same series of flashes as was used in the experiment in (**A**). The a-wave components of the responses of the $Nrl^{-/-}$ mouse in (**A**) have been extracted and normalized and fitted with a model of the activation phase of phototransduction (**C**),[18,19] modified to incorporate the membrane time constant,[22] which was set to 2 ms. The amplification constant obtained from fitting the model is A = 3.6 s^{-2} (cf. equation 1). (**D**) The a-wave components of the responses of the WT mouse (**B**) have been normalized and analyzed with the model, with a membrane time constant of 1 ms. The amplification constant of the same mouse obtained from fitting the cascade model to the a-wave responses to 500-nm flashes (data not shown) is A = 10 s^{-2}; the theory traces in (**D**) were obtained with this value of A, and a spectral sensitivity factor at 360 nm of S_{360} = 0.3. (**E**) Spectral sensitivities of the a-wave of $Nrl^{-/-}$ (●) and WT mice (○). Results such as those shown in (**C**) and (**D**) were analyzed as described in Lyubarsky et al.[15] to extract the spectral sensitivities. *Dark gray curve* through the $Nrl^{-/-}$ data was derived by combining a pigment template[69] having λ_{max} = 360 nm and unit sensitivity with a second template with λ_{max} = 508 nm and maximum sensitivity of 0.08; *dashed curve*: 360-nm template alone. The *light gray curve* through the rod data (○) is a 500-nm template above 470 nm and a fifth-order spline below 470 nm. The rod data and template curves are taken from Lyubarsky et al.[15] (**F**) The saturating amplitude a_{max} of the a-wave of $Nrl^{-/-}$ mice as a function of age,

derived from experiments such as illustrated in (**A**). Each point is the mean ± SEM of a group of 6 to 10 mice (except the initial point, for which $n = 5$) and is plotted at the mean age of the group. For each mouse the responses from both eyes to at least 5 (but up to 20) saturating flashes were averaged to estimated a_{max}. *Gray rectangles* identify two groups of mice: average age 39 days (*top left;* $n = 33$); average age 104 days (*bottom right;* $n = 13$). The difference in a_{max} between these two groups was significant at $P < 10^{-9}$ (two-sample *t*-test, $df = 35$).

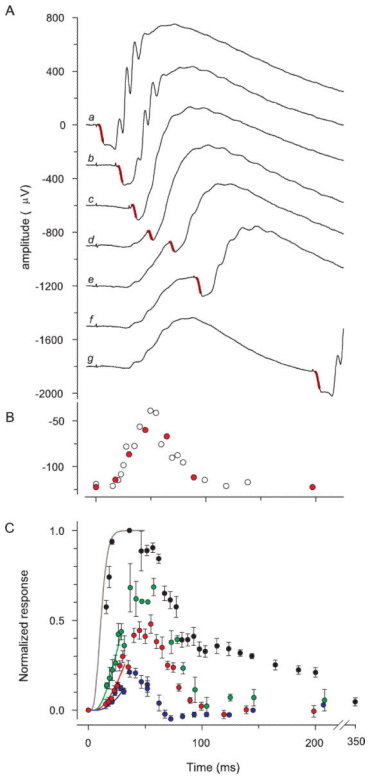

Figure 7.

Kinetics of the photocurrent response of the $Nrl^{-/-}$ mouse derived with the paired-flash ERG method. (**A**) Series of traces (b–g) from experiment in which a single 360-nm test flash was delivered at $t = 0$ followed by an intense probe flash that saturated the a-wave amplitude. Trace a: response to the probe alone, delivered at $t = 0$; trace g: an almost complete response to the test flash. The portion of the traces highlighted in *red* is the a-wave component of the response to the probe flash, and gives a measure of the residual photoreceptor circulating current present at various times after the test flash (i.e., that not suppressed by the test flash). Each trace is the average of 7 repetitions of a series of 24 combinations of the test and probe flashes. (**B**) Amplitudes of the responses to the probe flash in the experiment of (**A**), plotted as a function of the time of its delivery; *red symbols*: amplitudes derived from the seven traces illustrated in (**A**); *open symbols*: other data collected at other test–probe intervals in the same experiment. (**C**) Results from paired-flash experiments involving 360-nm test flashes of different strengths. The intensities (in photons per square micrometer at the cornea) and number of animals (*n*) whose data were averaged were 3,900 (11, *blue symbols*), 7,300 (6, *red symbols*), 23,300 (6, *green symbols*), 40,000 (3, *black symbols*). The smooth curves are derived from the activation model of photo-transduction with $A = 7.5\ s^{-2}$. The curves are color coded in correspondence to the respective sets of data.

Table 1

Features of *Nrl*$^{-/-}$ Photoreceptors Compared with Those of WT Mouse Rods and Cones

Feature	*Nrl*$^{-/-}$ Photoreceptors	WT Cones	WT Rods	Figure (Current Study)
Ultrastructure				
OS length (μm)	7.3 ± 1.3 (21)	13.4 ± 0.7*	23.6 ± 0.4*	Fig. 2
OS width (μm)	1.2 ± 0.3 (21)	1.2 ± 0.03*	1.4 ± 0.1*	Fig. 2
OS volume (μm^3)	8.3	14	36	
Open discs	up to 30	>15*	5-7*	Fig. 2
Mitochondrial length (μm)	0.94 ± 0.38 (50)	1.31 ± 0.7 (13)*	2.20 ± 0.7 (15)	Fig. 2
Histological				
Chromatin clumping	Yes	Yes	No	Fig. 1
PNA-stained OS sheath	Yes	Yes	No	Fig. 3
Molecular				
MUV	Yes	Yes	No	Figs. 3-5
$G_t\alpha 2$	Yes	Yes	No	Fig. 5
mCarr	Yes	Yes	No	Fig. 5
Arrestin	Yes†	Yes, low level‡	Yes	
ERG a-wave				
λ_{max} (nm)	360	360	500	Fig. 6
t_{peak} (ms)	≈50	unknown	140§	Fig. 7

The first column gives a list of the features on which *Nrl*$^{-/-}$ photoreceptors, WT rods, and WT cones are compared. Entries summarize data from this investigation or from previously published work. Error terms are standard deviations; numbers following in parentheses give sample size.

*Carter-Dawson and LaVail.[28]

†Mears et al.[5]

‡Craft and Zhu, personal communication, 2004.

§Hetling and Pepperberg,[41] who used the paired-flash method to extract rod responses from WT mice, as was used in the present study in *Nrl*$^{-/-}$ mice.